Fermi surface determination on LaV_2Al_{20} by using pulsed high magnetic fields

Kenji Mochidzuki, Hishiro T. Hirose

Abstract

Fermi surface determination on LaV_2Al_{20} that shows large diamagnetic response has been conducted by measuring quantum oscillations in pulsed high magnetic fields. Measurment of the quantum oscillations with large intensities was succeeded along [111], while it was hard to measure the quantum oscillations of fundamental frequencies along [001] due to a happening of magnetic breakdown. As a result of our experiments, it was revealed that a small hole-like Fermi surface has thinner rod-like shape than that estimated by an ab initio calculation and has a cyclotron effective mass as small as 0.067(1)–0.57(9) times that of free electron mass. These features suggest that the large diamagnetic response of LaV_2Al_{20} mainly originates in this small hole-like Fermi surface. In addition, it would be possible to measure the quantum oscillations and extract informations about large Fermi surfaces on heavy fermion compounds ReV_2Al_{20} (Re is rare earth element) using the same measurement environments.

1. Introduction of authors

Kenji Mochidzuki:

The major is the solid state physics, especially measurements of physical properties in high magnetic fields on strongly correlated conducting systems and developments of instruments used in pulsed high magnetic fields. In this study, his contributions are in the developments of rotating probe with non-metallic materials and in the measurement in the pulsed magnetic field.

Hishiro T. Hirose: The major is the solid state physics and chiemistry. He is attracted to the beauty of single crystals and the various physical properties of solids. He discusses the physics of solids by measuring the physical propertis of single crystalline samples synthesized by him. In this study, he contributed to synthesize the single crystalline sample of LaV_2Al_{20} and to analyze the measured quantum oscillations.

2. Origin and purposes of this study

LaV_2Al_{20} is an intermetallic compound with $CeCr_2Al_{20}$-type crystal structure.[1)] While a series of compounds with similar formulae as AV_2Al_{20} (A = Ga_x, Al_x, Sc_x, Lu) shows a conventional paramagnetic response, LaV_2Al_{20} shows a large diamagnetic response.[2)] This is why the electron states of LaV_2Al_{20} are interesting. The estimation of the electron states has been conducted by measuring the quantum oscillations at 2 K up to 10 T of magnetic field.[3)] It pointed out that an small hole-like Fermi surface can possibly produce a large Landau-Peierls diamagnetic response. However, in this measurement, only information on the small Fermi surface consisting of ~1% of carriers has been obtained due to the difficulty to synthesize the single crystal with high purity. The electron states of larger Fermi surfaces, containing rest 99% carriers, are still unknown. To discuss the characteristics of the small Fermi surface, it is neccesary to experimentally determine the whole electron states including the large Fermi surfaces, and thus the measurement of quantum oscillations under the condition of lower temperature and/or higher magnetic field are desired. Therefore we reached an idea that a

non-distructive pulsed magnet in Kindo laboratory at ISSP, the University of Tokyo could measure the quantum oscillations of non-high purity LaV_2Al_{20} single crystal with enough intensities to determine the whole electron states.

Another purpose of this study is related to the compounds having the same crystal structure as that of LaV_2Al_{20} and having rare earth element (*Re*) instead of La, which show interesting phenomena coming from hybridization between 4*f* and conducting electrons. Especially, PrV_2Al_{20} is known to locate near the quantum critical point counterbalanced with the Kondo effect and the RKKY interaction and to exhibit the quantum critical phenomena originated in the orbital degree of freedom.[4, 5] If one could measure the quantum oscillations on these compounds, it would be possible to experimentally determine their strength of electron correlation from the increasing ratio of effective mass from LaV_2Al_{20}. However, it is also difficult to synthesize the single crystal of ReV_2Al_{20} with high purity. Because they would have heavier effective mass than LaV_2Al_{20} due to the electron correlation, it requires even severer condition (lower temperature and/or higher magnetic field) to measure the quantum oscillations. The key point is that the sufficient condition to measure the quantum oscillations of ReV_2Al_{20} is still unclear. The experience to determine the whole electron states of LaV_2Al_{20} through measuring the quantum oscillations under the high magnetic field would be precious information to estimate the sufficient condition.

Thus, we measure the quantum oscillations of LaV_2Al_{20} (i) to clarify the characteristics of the small hole-like Fermi surface by experimentally determining the whole electron states of LaV_2Al_{20} and (ii) to give information to estimate the sufficient condition for the measurement of quantum oscillations on ReV_2Al_{20} having heavy fermions.

3. Method

In this section, we provide the detail of a single crystal of LaV_2Al_{20}, a nondestructive pulsed magnet, and a rotation probe for rotating the sample in pulsed magnetic fields. Moreover, we explain the method of a contactless resistivity (TDO) measurement used for the observation of the Shubnikov-de Haas (SdH) oscillation in LaV_2Al_{20}.

3.1 Single crystalline sample of LaV_2Al_{20}

A single crystalline sample of LaV_2Al_{20} was prepared by the self-flux method, and the *RRR* of the sample was about 11. We can consider that the purity of the sample is good enough to measure the SdH oscillation, since the de-Haas van Alphen oscillation has been observed by using the same sample as that used in this study.[3] Figure 1 shows the picture of the sample. LaV_2Al_{20} forms a regular octahedron type crystal, which characterizes the cubic crystal, and the regular triangle plane of the crystal corresponds to the very flat (111) plane. The direction of the magnetic field for the crystal orientation was defined as Fig. 1(b). For the symmetry of the crystal, we can conduct the full Fermi surface scan by measuring quantum oscillations for two different rotations, θ rotation ([001]→[111]→[110]) and ϕ rotation([001]→[101]).

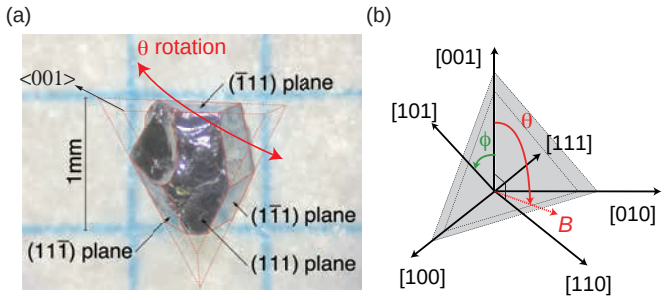

Fig. 1 (a) Picture of the single crystalline LaV_2Al_{20} (b) Angle definition of θ, ϕ.

3.2 Nondestructive pulsed magnet

Pulsed magnets enable us to reach the magnetic fields over 50 T because of a short duration time less than 1s. In this work, we used a nondestructive pulsed magnet developed at Kindo laboratory, ISSP, the University of Tokyo. The cross section of the magnet and the waveform when the maximum magnetic field of this magnet is generated are shown in Fig 2(a, b), respectively. This magnet can be characterized by following two points. One is that a multi-layer solenoid coil is wound by using Cu-Ag alloy wires several times stronger than normal Cu wires, and the other is that maraging steels with high strength reinforce the solenoid coil. Owing to those, the pulsed magnet can generate magnetic fields up to 56 T without the destruction by the Maxwell stress (~1.4 GPa @ 60 T[6]) caused by self magnetic fields.[7,8] The power supply for generating magnetic fields is a large capacitor bank (18 mF, 10kV, 900 kJ). To generate a 56 T magnetic field, the energy of 730 kJ (9kV charging) is discharged to the pulsed magnet for 38 ms.

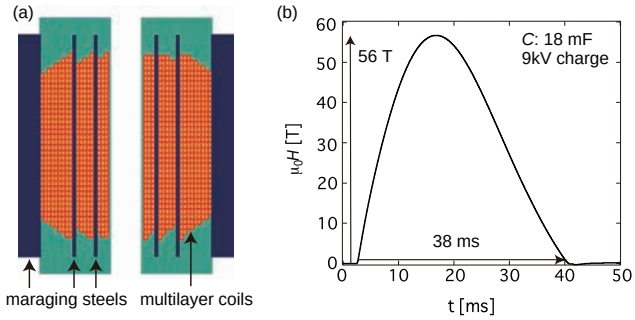

Fig. 2 (a) Pulsed magnet developed at Kindo laboratory (b) Profile of a 56 T pulsed magnetic field.

3.3 Sample probe with a nonmetallic and nonmagnetic rotator

For scanning the Fermi surface of LaV_2Al_{20}, it is necessary that the sample should be rotated to vertical magnetic fields precisely. Thus we prepared the rotation probe shown in Fig. 3(a). The rotation part (Swedish gear) of this probe shown at the lower left side of Fig. 3(a) was made of PEEK (PolyEtherEtherKetone) for preventing from the Eddy current heating. The other parts were made of stainless steels (SUS304) since it can be easily processed (cutting, welding, and so on). The Swedish gear can be rotated by 10 degrees per one rotation of the stainless rod which extends to the top of the probe (see blue arrow at the lower right side of Fig. 3(a)). The magnetic fields and rotation angles are detected by using pick-up coils. Although the angle detection coil wound up parallel to the sample platform is invisible in Fig. 3(a), it is put on the backside

of the platform. Therefore the induced voltage of the angle detection coil oscillates with the same cycle of the platform rotation. By measuring the voltage, we can get the angle between the magnetic field and the sample. Figure 3 (b) shows the picture of the sample platform with the sample attached (θ rotation). The sample was fixed by using electric insulating GE-varnish. Since the GE-varnish can be easily dissolved by acetone, we can attach the sample at the appropriate angle finely. The sample temperature was measured by using a resistance thermometer (Cernox) which is put close to the sample. The rotation part and the sample are inserted into a cryostat for liquid ^{4}He that maintains the low temperature of 4.2 K. Moreover we can achieve the lower temperature down to 1.3 K by pumping the liquid ^{4}He in the cryostat. The temperature control can be done by changing the pressure in the cryostat below 4.2 K. On the other hand, above 4.2 K, we do not actively control temperature by using a heater because the heater often causes the local temperature gradient.

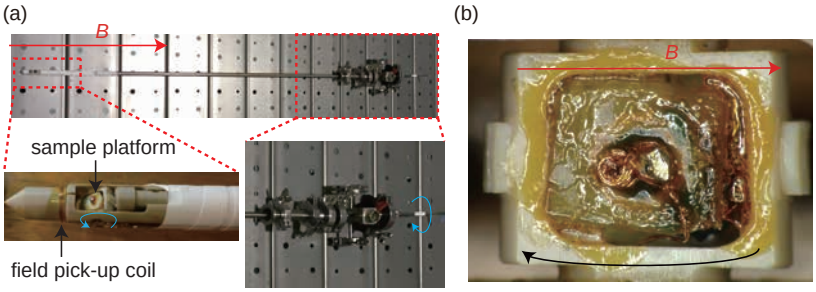

Fig. 3 (a) Picture of the rotation probe for pulsed magnetic fields (b) Sample platform with the sample attached (θ rotation: <001>→<110>).

3.4 Tunnel Diode Oscillator (TDO) measurement

Tunnel Diodes (TD) have been introduced by L. Esaki in 1957, and those have a negative resistance region in a forward voltage operation.[9] Owing to this character the TD can compensate the energy loss yielded by the circuit resistance so that it enables to stabilize the resonance of the *LC* oscillator circuit as shown in Fig 4(a). TDO measurement is a contactless method that allows us to measure the resistivity change of the sample put in the transmitting coil by using the oscillator circuit (~100 MHz) with the TD. [10]

When the *LC* circuit is resonant, the resonance frequency f can be written as $1/2\pi(LC)^{1/2}$, where the C, L are the capacitance of the capacitor and inductance of the coil in the circuit, respectively. Assuming that the capacitance is constant (i.e. independent of temperature and magnetic field), the resonance frequency is changed by the inductance. The inductance will be changed if a sample is inserted into the coil which plays the inductance part in the circuit. For example, it is well known that in case that a metallic sample is inserted into the coil, the skin effect of the sample interacts with the inductance of the coil, and as a result the change of the resonance frequency Δf is proportional to that of the skin depth $\Delta\delta$ of the sample [11]

$$\Delta f \propto \Delta \delta . \qquad (3.1)$$

In addition, the skin depth is proportional to the square root of the sample resistivity $\rho^{1/2}$. Consequently the resonance frequency can be written as

$$\Delta f \propto (\Delta \rho)^{1/2}. \qquad (3.2)$$

Thus the TDO measurement enables to observe the change of the sample resistivity without any electric contacts with the sample. This method is powerful way to measure a periodic change of the resistivity like as a quantum oscillation although it is inconvenient way to obtain the absolute value of the sample resistivity. Since the sample resistance is not measured directly, this method can be applied to very low resistivity samples without special sample fabrications.

Figure 4(b) and (c) shows the picture of the resonance circuit with a TD and resonance coil, respectively. For stabilizing the resonance[11], several capacitors and resistances are contained in addition to the simplest resonance circuit shown as Fig. 4(a). The almost all parts of the circuit shown in Fig. 4 (b) were put in the room temperature space but the only resonance coil connected with a semi-rigid coaxial cable was laid in the cryostat. To prevent from the excess bias voltage caused by a rapid field sweep of the pulsed magnet, we employed the 8-shaped coil (Fig. 4(c)).

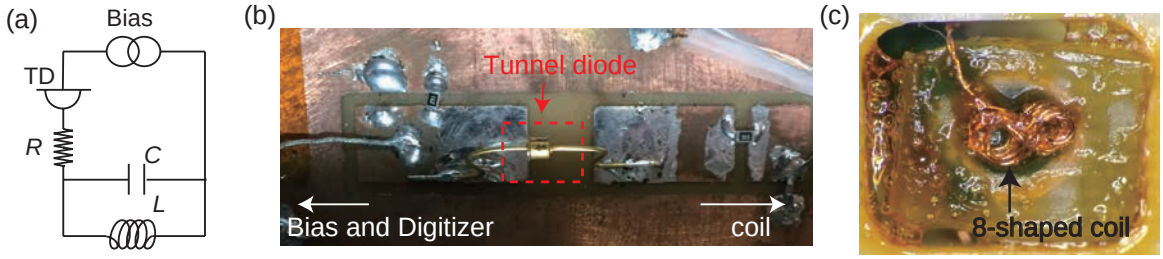

Fig. 4 (a) Simplest LC resonance circuit with a TD (b) Resonance circuit with a TD used in this work actually (room temperature part) (c) 8-shaped resonance coil for pulsed magnetic field (low temperature part).

4. Analysis

The SdH oscillations overimposed on the magnetic field dependence of resonant frequency is analyzed as described below. The basic points on SdH oscillations, how to extract the component of SdH oscillations by subtracting a background from raw data, tequnique to reduce the influence of noize coming from the measurement environment, and details about the calucuration of electron states used to compare with experimental results are explained.

4.1 Shubnikov-de Haas oscillation

SdH oscillation is a quantum oscillation of an electric conductivity.[13] In a magnetic field, conduction electrons are in discrete energy levels called Landau levels. Both the energy gap between adjacent Landau levels and the number of degenerate states at each Landau levels are proportional to the magnetic field B. As a result, the dencity of states at the Fermi energy oscillates versus the inverse of B. The change of the density of states at the Fermi energy leads to the change of the scattering probability of conduction electrons, and hence the electron conductivity changes. That is why SdH oscillation appears. Although it is hard to exactly formulate the SdH oscillation, the oscillating part of an electron resistivity $\Delta\rho$ can be described as below with a lot of approximation,

$$\Delta\rho \propto \Sigma_i A_{\rho,i} \cos[2\pi\nu(F_i/B - 1/2) \pm \pi/4]. \qquad (4.1)$$

Here, A_ρ and F are the amplitude and the frequency of SdH oscillation, respectively, and ν is an integer. An oscillation with $\nu = 1$ is of a basic wave and the one with $\nu > 1$ is a harmonic wave. The observation of the harmonic wave is more difficult

than that of the basic wave because the A_ρ becomes small with the increasing of ν. From the relation of Onsarger,[13] the frequency is expressed as $F = \hbar S_{ex}/2\pi e$ using an extremal cross section of the Fermi surface perpendicular to a magnetic field S_{ex}. By measuring the variation of S_{ex} versus magnetic field direction, it is possible to experimentally obtain a rough shape of the Fermi surface. On the other hand, from the temperature dependence of the A_ρ, we can get the cycrotron effective mass m_{cyc} since it is well known that in the case of the quantum oscillation in the electric resisitivity the T dependence of A_ρ is described as

$$A_\rho \propto \lambda/\sinh \lambda \qquad (4.2)$$

$$\lambda = 2\pi^2 \nu k_B T m_{cyc}/e\hbar B. \qquad (4.3)$$

In the TDO measurement, by using formula (3.2),

$$A_{TDO} \propto A_\rho^{1/2} \propto (\lambda/\sinh \lambda)^{1/2}. \qquad (4.4)$$

Thus by examining the T dependence of A_{TDO}, m_{cyc} of a Fermi surface can be determined.

4.2 Extraction of the oscillating components

Figure 5(a) shows the magnetic field dependence of the change of resonant frequency Δf measured at $T \sim 1.4$ K for $B \parallel$ [001]. The up sweep data Δf^{up} and down sweep one Δf^{down} is represented as yellow and blue lines, respectively. Both Δf^{up} and Δf^{down} decrease with increasing B. This is because of the magnetoresistance of the sample and the pickup coil. As shown in the inset of Fig. 5(a), the common oscillating component superimposed on Δf^{up} and Δf^{down} appears in high field region. This oscillation is the SdH oscillation of LaV_2Al_{20}. To extract the component of SdH oscillation Δf_{SdH}, the background Δf_{BG} is approximated as 3D spline curve[14] and subtracted from the measured Δf. 3D spline curve is a curve that seamlessly connects between adjacent control points with third polynomial function. To obtain Δf_{BG}, firstly the abscissa and number of control points are set not to include the component of SdH oscillation as part of the background, and secondly determine the ordinate of control points by the least square method. Shown in Fig. 5(b) are the background Δf_{BG}^{up}, the position of control points and the component of SdH oscillation Δf_{SdH} determined for up sweep Δf^{up} shown in Fig. 5(a).

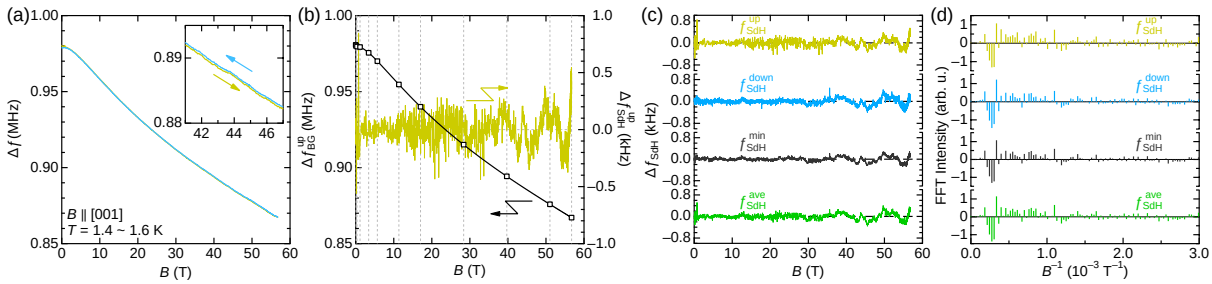

Fig. 5 (a) Magnetic field dependence of the change of resonant frequency of LaV_2Al_{20} measured at 1.4 ~ 1.6 K in a magnetic field along [001]. Inset shows the expansion of the higher field region. Arrows indicate the up sweep or down sweep. (b) Magnetic field dependence of the background (left axis) and the component of SdH oscillations (right axis) obtaind for up sweep. The former is in a form of 3D spline curve whose control points are shown as squares and the latter

is determined by substituting the former from the raw data. (c) Magnetic field dependence of SdH oscillations. (d) Real part of the FFT spectra on the SdH oscillations versus magnetic field *B*. Components of SdH oscillations for up sweep Δf_{SdH}^{up} and down sweep Δf_{SdH}^{down} , their average Δf_{SdH}^{ave} and their common component Δf_{SdH}^{min} are shown in (c) and (d).

4.3 Analysis of oscillating components

Because a SdH oscillation is an oscillation versus an inverse of magnetic field, the frequency and the intensity of the oscillation are obtaind by Fourier transforming a component of SdH oscillation versus an inverse of magnetic field. Figure 5(c) shows the magnetic field dependences of the components of SdH oscillations for up sweep Δf_{SdH}^{up} and down sweep Δf_{SdH}^{down} from the raw data in Fig. 5(a). While there are common components of SdH oscillations, we can find superimposed unnegligible noise originated in the measurement environment especially on 10 ~ 30 T of Δf_{SdH}^{up}. Because the frequencies of the noise are close to that of the SdH oscillations, they could be obstacles in the examination of the fast Fourier transformed (FFT) spectra. To distinguish the component of SdH oscillations from the noise, we used two techniques taking advantage of the noise appearing differently in Δf_{SdH}^{up} and Δf_{SdH}^{down}.

The one is simply calculating the average of Δf_{SdH}^{up} and Δf_{SdH}^{down}. The averaging reduce the influence of the noise by a factor of $2^{-1/2}$. The averaged result Δf_{SdH}^{ave} shown in Fig. 5(c) represents that this technique is effective.

The other is extracting the common component of Δf_{SdH}^{up} and Δf_{SdH}^{down}. The real parts of the FFT spectra for Δf_{SdH}^{up} and Δf_{SdH}^{down} (Re[FFT(Δf_{SdH}^{up})] and Re[FFT(Δf_{SdH}^{down})], respectively) are shown in Fig. 5(d). Synthesize the spectrum taking absolutely smaller value for real and imaginary parts from each frequency of Δf_{SdH}^{up} and Δf_{SdH}^{down}. The oscillation Δf_{SdH}^{min} produced by inversely Fourier transforming this spectrum is shown in Fig. 5(c). It can be seen that the reduction of the influence of noise is larger in Δf_{SdH}^{min} than Δf_{SdH}^{ave} because the former only contains common component of Δf_{SdH}^{up} and Δf_{SdH}^{down}. In Δf_{SdH}^{min}, the SdH oscillations part is also reduced and hence the reliability on the intensity is lost. Instead, the accuracy on the frequency is increased.

In this study, we used the latter technique to evaluate the frequency and used the former one to evaluate the intensity.

4.4 Electron structure of LaV_2Al_{20}

To compare the information on the Fermi surfaces experimentaly obtained from the SdH oscillations with computationaly obtained one, we used the electron structures calculated by Prof. Harima in Kobe University. The code used in the calculation is called TSPACE and KANSAI-06, which employs full-potential linearized augmented plane wave method under the local density approximation. The crystal structural parameter used in the calculation is obtained by single crystalline X-ray diffraction measurement at 100 K on a LaV_2Al_{20} sample synthesized under the same condition with the one used in this study. This measurement and the analysis were done by Assoc. Prof. Yamaura in Tokyo Tech and Tech. Asst. Prof. Yajima in ISSP, Univ. of Tokyo.

5. Results and discussions

5.1 Estimation of the shape of Fermi surfaces by angular dependence

Magnetic field dependences of the components of SdH oscillations $\Delta f_{\mathrm{SdH}}^{\mathrm{min}}$ measured in various magnetic field directions are shown in Fig. 6(a). The direction of magnetic field is represented with θ or φ defined in Fig. 1(b). The SdH oscillations evenly spaced in B^{-1} scale exist in all directions, which vary with field angle. Figure 6(b) shows the FFT spectra of the SdH oscillations FFT($\Delta f_{\mathrm{SdH}}^{\mathrm{min}}$) between 35 and 55 T. Positions of the peaks in the FFT spectra correspond to the frequencies of SdH oscillations. Here, the region between 35 and 55 T corresponds to a period of F = 96.25 T, which is the resolution limit of this FFT spectra. Widening the FFT range to the lower magnetic field increases the resolution of the frequency and decreases the intensity of the peak and hence the peak becomes unclear. This is because an intensity of quantum oscillation becomes smaller in a lower magnetic field. To determine the value of frequency in the trade-off relationship between the resolution and the intensity, we picked up the best appropriate value from the FFT spectra between 20, 30, 35 or 40 and 55 T according to the frequency and intensity of each peak. The picked up frequencies are indicated in Fig. 6(b) by using arrows. It is worth mensioned that there are several peaks we didn't pick up such as the frequencies smaller than 200 T (too small to determine), multiple frequencies with nearly same values (hard to separately determine), and the frequencies only appear in particular FFT region (noise). The angle dependences of the obtained frequencies are shown in Fig. 6(c) according to θ or φ. The frequencies obtained from the ab init calculation are also plotted as gray symbols. The two hole-like Fermi surfaces FS1 and FS2 and one electron-like Fermi surface FS3 as the result of the calculation are shown in Fig. 7(a–c).

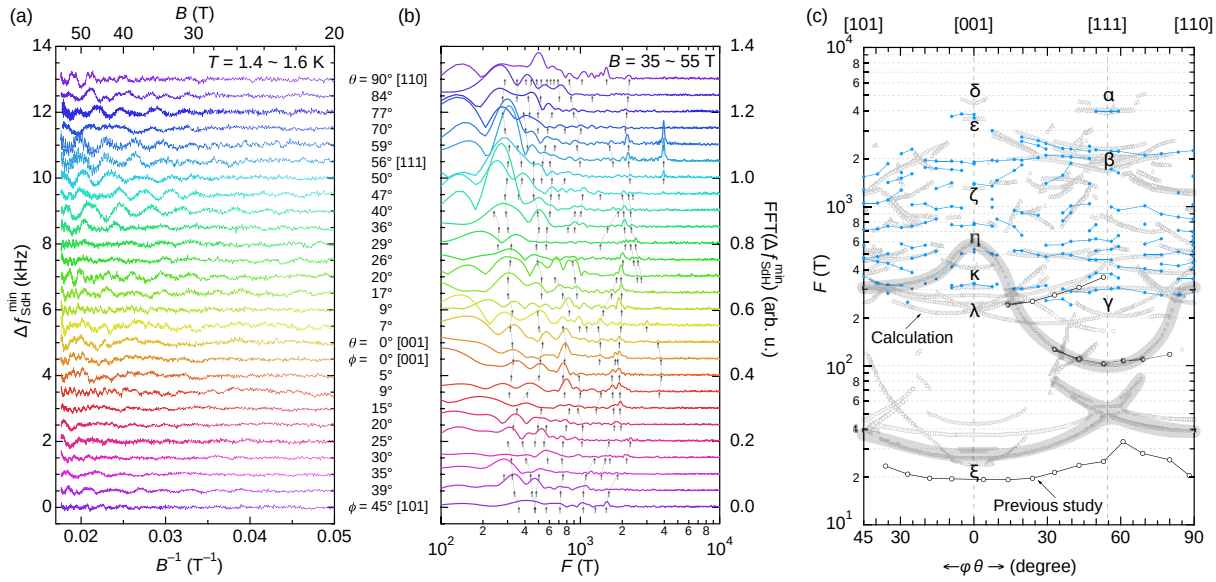

Fig. 6 (a) B^{-1} dependences of the components of SdH oscillations $\Delta f_{\mathrm{SdH}}^{\mathrm{min}}$ and (b) their FFT spectra between 35 and 55 T measured at 1.4–1.6 K on LaV_2Al_{20}. Magnetic field directions are represented by θ or φ defined in Fig. 1 (b). Arrows indicate the determined values of frequencies picked up from the appropriate FFT region for each frequency. (c) Observed frequencies versus magnetic field direction. Black empty circles indicate the frequencies of de Haas-van Alphen oscillations on torque measured in the previous study. Gray plots are expected frequencies from ab initio calculations. Gray markers emphasize the frequencies of FS1 shown in Fig. 7(a).

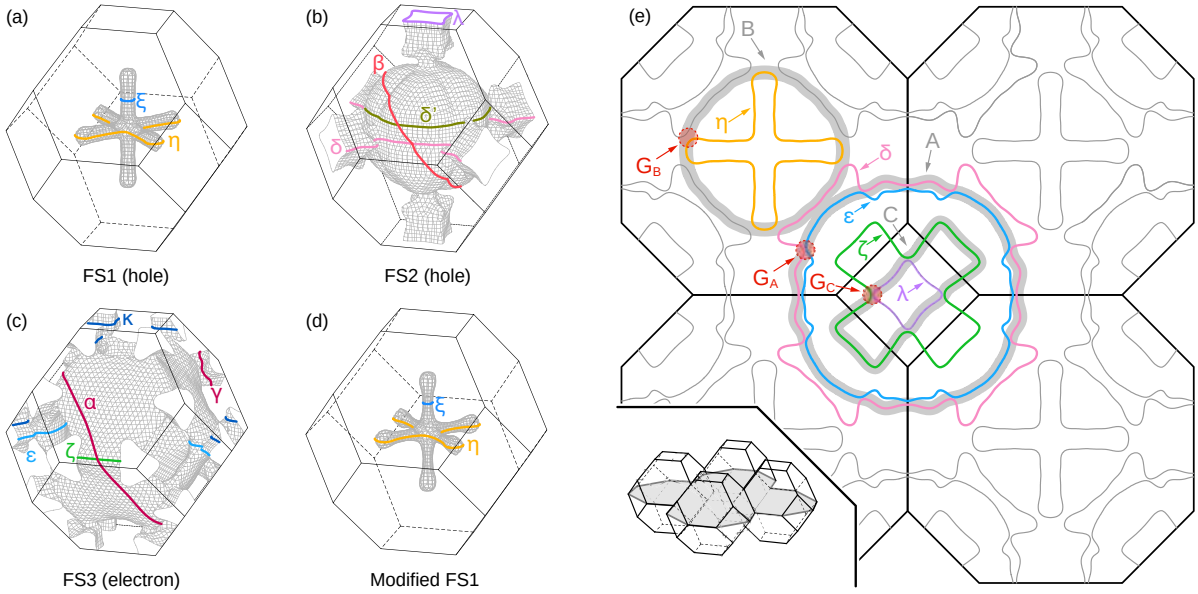

Fig. 7 (a, b, c) Three Fermi surfaces FS1 (hole-like), FS2 (hole-like) and FS3 (electron-like) expected from ab initio calculation. Typical orbits are represented as thick lines. (d) Revised shape of FS1 expected from the experimental results. (e) Cross-section drawing of the Fermi surfaces at a plane containing Γ points of the adjacent Brillouin zones (indicated as gray plane in the inset). Typical orbits are represented as thick lines. Typical gaps between adjacent orbits G_A, G_B and G_C are represented as red broken circles, and typical orbits A, B and C connected due to the magnetic breakdown at these gaps are represented as thick gray lines.

In B ∥ [111] direction (θ = 56°), both oscillations with the largest frequency of 3970 T and the small frequency of 304 T have large amplitudes. The orbits corresponding to the former and latter oscillations are α orbit and γ orbit on FS3, respectively. In the same field direction, the oscillation with a frequency of 2220 T also has large amplitude, which corresponds to β orbit on FS2. The amplitude of a SdH oscillation is proportional to the density of states at Fermi level of the corresponding band. Thus it is considered that the amplitudes of α, β, γ orbits are large because α and β orbits are of the large Fermi surface and γ orbit has high multiplicity. The field angle dependences of the frequencies of these orbits are small. As for the amplitudes, the amplitude of α orbit rapidly decreases and vanishes within ±5° range, whereas the ones of β and γ orbits are gradually decrease and vanish within ±30° range. Because these observed results are consistently explained with the result of ab initio calculation, it is indicated that both the hole-like FS2 and electron-like FS3 of LaV_2Al_{20} are well replicated by the calculation.

On the other hand, in B ∥ [001] direction (θ = 0°, φ = 0°), all experimental results do not coincide with the theoretical expectation. The frequency corresponding to η orbit on FS1 is 560 T, which is slightly smaller than 580 T expected from the ab initio calculation. This correspondence is confirmed by the coincidence of the φ dependence of experimental and calculation frequencies between 0° and 20°. In addition, the frequency expected as κ orbit on FS3 is 320 T, which is near the expectation of the ab initio calculation. However, the frequencies corresponding to other typical orbits expected from the ab initio calculation are not observed or significantly discrepant. For example, in high frequency region, 4407 T of δ

orbit and 3463 T of ε orbit are expected although only an oscillation with 3810 T with tiny amplitude is observed in this region. In addition, 1220 T of ζ orbit is expected although the nearest observed frequency is 1400 T. Furthermore, instead of these frequencies, oscillations having large amplitude with frequencies of 786 T, 1780 T and 1910 T are observed, although they aren't expected from ab initio calculation.

These discrepancies are due to the occurence of the magnetic breakdown (MB). The MB is a phenomenon that an electron, which basically moves along the orbit on one Fermi surface, goes around a large orbit that the adjacent Fermi surfaces are combined. This is caused by that an electron with a large kinetic energy jumps a small gap which separates between the bands in a finite probability.[13] Under the high magnetic field, the kinetic energy of the cyclotron movement becomes large, hence the probability of jumping a gap p becomes large and the occurence of MB get easier. Figure 7(e) shows the cross-sections of the Fermi surfaces at the plane containing Γ points of adjacent zones in the extended Brillouin zone shown in the inset. There are δ, ε, ζ, η, λ, and ξ orbits on the three Fermi surfaces, FS1, FS2 and FS3 expected with B || [001] direction. Here, three couples of orbits, δ and ε, δ and η, and ζ and λ are adjacent in the reciprocal space and have small separation gaps G_A, G_B, and G_C, respectively. When MBs happen at these gaps, electrons go around on the different orbit that consists as jointing the original orbits at the jumped gap, and SdH oscillation with the frequency corresponding to the new orbit appears. The expected MB orbits A, B and C when MB happens at G_A, G_B and G_C are exemplified as thick gray line in Fig. 7(e). Because p is finite (never reaches 1), there is a variety of MB orbits depending on with or without jumping at each gap in an orbit.

Figure 8 exemplifies main six patterns of C orbits depending on the p values and with or without jumping G_C gaps. Note that if you consider even less probable orbits with and without MB, there are infinite varieties of C orbits. The corresponding frequency of the MB orbit is also proportional to the area surrounded by the orbit. Thus, as for C orbits, ζ orbit of 1220 T and λ orbit of 213 T are expected to mainly produce four new MB orbits of three frequencies, 466 T, 718 T and 970 T. The corresponding amplitude of each MB orbits is proportional to $p^j(1-p)^k$, where j and k are numbers of times jumping and not jumping gaps in a period, respectively.[13] Based on this principle, the frequencies observed in B || [001] could be understood as follows.

First of all, the observed frequency of 786 T is considered as (1/2) ζ + (1/2) λ orbit of C orbits, whose frequency is expected as 718 T. On another front, the frequencies 466 T and 970 T corresponding (1/4) ζ + (3/4) λ and (3/4) ζ + (1/4) λ, respectively, aren't observed. This fact indicates that p is close to 1 and MB is highly probable at the gap of G_C. If so, it is highly probable that the observed frequency of 1400 T would be not corresponding to ζ orbit, but to the second harmonic oscillation (ν = 2) of (1/2) ζ + (1/2) λ orbit.

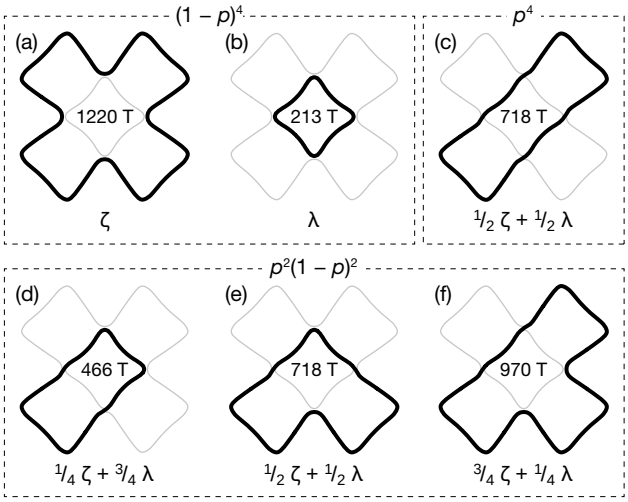

Fig. 8 Typical six variations of orbits produced by magnetic breakdown from ζ orbit and λ orbit are shown as thick line. The corresponding frequencies are written at the center of orbits. The gray thin lines are ζ orbit and λ orbit. The orbits are categolized with broken lines based on the coeficient on oscillating amplitudes, which considering the effect of *p*, a probability to jump the gap G_C.

Secondly, the observed frequency of 3810 T is considerd to correspond to A orbit shown in Fig. 7(e), which is expected to have the frequency of 3743 T. Because A orbit has 8 gaps in a period, the reduction due to MB is large and hence the amplitude is small. This orbit is also expected only when *p* is close to 1, which is consistent with the fact that oscillations of δ orbit and ε orbit without MB are not observed.

Lastly, the observed frequency of 1780 T is considered to correspond to B orbit shown in Fig. 7(e), which consists of δ orbit and η orbit and is expected to have the frequency of 1707 T. The area surrounded by B orbit is the local minimum value because B orbit is along the ditch on FS2. Thus, there is the local maximum value of cross-section area of FS2 where cross-section plane is slightly shifted perpendicularly from the plane shown in the inset of Fig. 7(e). The orbit corresponding this local maximum cross-section area, δ' orbit, is expected to correspond to the observed frequency of 1910 T. As the direction of magnetic field inclines, δ' orbit continuously leads to β orbit along *B* || [111]. This is consistent with the fact that the observed frequency shows the continuous angle dependence from 1910 T in *B* || [001] to 2220 T in *B* || [111]. It must be mentioned that because MB produces B orbit from δ orbit and η orbit, the amplitude of observed oscillation corresponding to η orbit is considered to have some reduction for it.

As mentioned over the three paragraphs, the origin of SdH oscillations in *B* || [001] direction could be understood by considering MB orbits of A, B and C.

It is difficult to discuss the detailed shapes of Fermi surfaces based on the MB orbits. However, because almost all observed frequencies could be understood by the results of ab initio calculation and the expected MB orbits, the results of ab initio calculation for large Fermi surfaces seems to be very close to the real electron states. As for small Fermi surface FS1, we could fortunately succeed to obtain the rough value of the frequency for η orbit in spite of the occurence of MB. η orbit corresponds to the maximum cross-section of the FS1. As mentioned above, the observed frequency of 560 T is

slightly smaller than 580 T expected by the result of ab initio calculation. In the previous study, the frequency corresponding to ξ orbit at the minimum cross-section of the pillar part of FS1 is confirmed as 19 T, which is smaller than 26 T expected from the ab initio calculation.[3] Considering these results, the real shape of FS1 is supposed to have thinner neck as shown in Fig. 7(d).

5.2 Estimation of the cyclotron effective mass by measuring the temperature dependence

From the temperature dependence of the amplitudes of SdH oscillations, m_{cyc}'s for η orbit and κ orbit can be estimated. Figure 9(a) shows the B^{-1} dependence of the component of SdH oscillation Δf_{SdH}^{ave} in B || [001] (θ = 0°, φ = 0°) at temperatures between 1.4 and 18 K. The positions of antinodes in the SdH oscillation of 560 T corresponding to η orbit are indicated as broken lines. The FFT spectra of the oscillatory components between 35 and 55 T are shown in Fig. 9(b). It could be seen that almost all peaks corresponding to κ, η and 1/2 ζ + 1/2 λ orbits decrease with increasing the temprature. The temperature dependences of amplitudes of the orbits without MB, η and κ, are shown in Fig. 9(c). They tend to decrease with increasing the temperature. By fitting these temperature dependences with formula (4.4), cyclotron effective masses for η orbit and κ orbit are obtaind as m_{cyc}/m_e = 0.57(9), 0.74(11), respectively. This value of η orbit on FS1 is about 8.5 times larger than m_{cyc}/m_e = 0.067(1) obtained for ξ orbit on FS1 in the previous study[3], but still smaller by half than that of the free electrons.

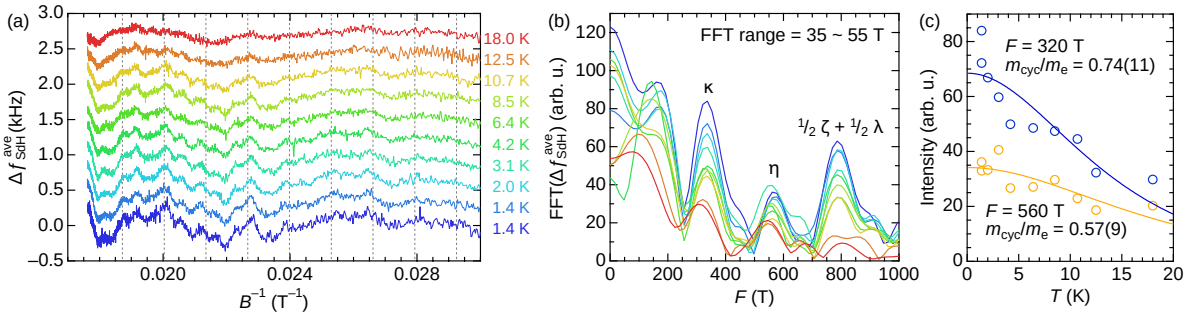

Fig. 9 (a) Temperature dependences of the SdH oscillation components Δf_{SdH}^{ave} versus magnetic field in B || [001] direction. Data of each temperature is equally shifted. Both upsweep and down sweep data only for 1.4 K are shown. The antinode positions of the SdH oscillation with 560 T frequency originated in η orbit are represented by broken lines. (b) Temperature dependence of the FFT spectra for Δf_{SdH}^{ave} between 35 and 55 T. (c) Temperature dependences of the oscillatory amplitudes (peak intensities of the FFT spectra) for κ orbit with the frequency of 320 T and η orbit with the frequency of 560 T. The solid lines indicate the results of fitting with formula (4.4).

The fact that m_{cyc} of η orbit is smaller than that of κ orbit having smaller cross-section area strongly represents the special feature of FS1. The cyclotron effective mass is defined as $m_{cyc} = \hbar^2/2\pi \times \partial S/\partial E$, where S is the area surrounded by the electron orbit in the reciplocal space. In general, in an large Fermi surface, the orbit with small S as of around the neck part tends to have smaller m_{cyc} than the orbit with large S because of the hybridization effect with adjacent bands.[15] For instance, in the electron-like Fermi surface of aluminum, γ orbit with the local maximum cross-section area has m_{cyc} 1.1–

1.9 times as heavy as that of α orbit with the local minimum cross-section area.[16] Therefore the fact that m_{cyc} of η orbit is smaller than that of κ orbit indicates that FS1 tends to have extremely light m_{cyc} than FS3 which has a large number of carriers. In addition, the shape of FS1 has the characteristic that the ratio of the surface area (density of states at Fermi level) to the volume (number of carriers) is notably large. Because the magnitude of Landau-Peierls diamagnetism is inversely proportional to the effective mass and proportional to the density of states at Fermi level,[17] it is supposed that (i) the extremely small effective mass among all electron carriers and (ii) the special shape with large surface/volume ratio in FS1 would be the origin of the large Landau-Peierls diamagnetism in LaV_2Al_{20}.

In our experiments of measuring the temperature dependence, it couldn't be accomplished to estimate the m_{cyc} of FS2 due to the occurence of the MB. However, because the amplitude of β orbit in B || [111] is especially large, m_{cyc} of FS2 is estimated as relatively small. Thus, it will be hasty to almost all of the diamagnetism in LaV_2Al_{20} originates in FS1. As an after work, I would like to precisely estimate the Landau-Peierls diamagnetism produced by only FS1 by using the value of m_{cyc}'s and the shape of the Fermi surface obtained in this study.

5.3 Toward the measurement of SdH oscillations in the heavy fermion system ReV_2Al_{20}

In this study, we measured the temperature dependences of SdH oscillations in B || [001] to determine the m_{cyc} of each Fermi surfaces. However, due to the occurence of MB, only m_{cyc} values of η orbit and κ orbit could be determined. It is espescially regretful to miss the m_{cyc} values of large orbits of δ and ε. On the other hand, in B || [111], it is expected that determining m_{cyc} values of main Fermi surfaces of the both of electrons and holes is relatively easier because both α orbit and β orbit show large intensities of SdH oscillations. Since there is no occurence of MB among main orbits in this magnetic field direction, we can consider that the direction of B || [111] is well suit for measuring SdH oscillations and its temperature dependences. Besides, because it is possible to measure the temperature dependence of SdH oscillations with enough intensities even with the sample of RRR = 11, it is expected as possible to measure the SdH oscillation even with increased effective mass up to ~50 times at the lowest temperature of 1.8 K. Note, however, that if the increase of effective mass is more than ~10 times, it is required to increase the purity of sample or accuracy of the measurement for obtaining the temperature dependences of the SdH oscillations. As an example of measuring the quantum oscillations of ReV_2Al_{20} (*Re* is rare earth element), there is a report to measure the SdH oscillations of PrV_2Al_{20}.[18] In this report, a value of m_{cyc}/m_e = 4.9 (1.9) for the oscillation with frequency of 250 T is obtained in the magnetic field along 75° from [111] to [1-21]. However, an oscillation with the frequency higher than 250 T isn't observed. Assuming that value of m_{cyc}/m_e in B || [111] was almost same as ~4.9, it would be possible to measure the SdH oscillation of PrV_2Al_{20} in this direction with the same measurement condition used in our study. Therefore, it is expected to reveal the electron states of PrV_2Al_{20} in the future study.

6. Summary

Shubnikov-de Haas (SdH) oscillation of LaV_2Al_{20} is measured in pulsed high magnetic fields. The analized results of SdH oscillations revealed that the small hole-like Fermi surface has the thinner pillar parts in its shape than that of expected by

the ab initio calculation. The cyclotron effective mass of the orbit surrounding the maximum cross-section of this Fermi surface is obtained as 0.57(9) m_e. It is now clear that this Fermi surface has extremely smaller effective mass compared to the large electron-like Fermi surface. Because of the small effective mass and the characteristic shape of the large surface/volume ratio, this small Fermi surface can be considered as the origin of large Landau-Peierls diamagnetic response. Besides, it was found that the SdH oscillations of most of the orbits in B || [001] cannot be observed due to the occurence of the magnetic breakdown. In case trying to estimate the cyclotron effective mass of heavy fermion system of $Re$$V_2Al_{20}$ (Re is rare earth element) by measuring SdH oscillations, B || [111] direction is suitable. It is expected to elucidate the electron states of the compound with Re = Pr by using the same experimental environment in this study.

7. Aknowledgements

We would like to thank Prof. Koichi Kindo, Prof. Zenji Hiroi, Prof. Masatoshi Imada and Prof. Takahisa Arima for giving the permision to carry out this work and helpful discussions. We are also grateful to Asst. Prof. Yoshimitsu Kohama for lots of advice for the pulsed high field experiments. The calculated electron states used in this work are provided by Prof. Hisatomo Harima in Kobe University, Assoc. Prof. Jun-ichi Yamaura in Tokyo Institute of Technology and Asst. Prof. Takeshi Yajima in X-ray Laboratory of ISSP. Finally, we express our great gratitude to the MERIT program for giving this invaluable research opportunity and the financial support.

8. References

1) M. J. Kangas, D. C. Schmitt, A. Sakai, S. Nakatsuji, and J. Y. Chan, J. Solid State Chem. **196**, 274 (2012).

2) A. Onosaka, Y. Okamoto, J. Yamaura, T. Hirose, and Z. Hiroi, J. Phys. Soc. Jpn. **81**, 123702 (2012).

3) T. Hirose, Y. Okamoto, J. Yamaura and Z. Hiroi, J. Phys. Soc. Jpn. **84**, 113701 (2015).

4) A. Sakai and S. Nakatsuji, J. Phys. Soc. Jpn. **80**, 063701 (2011).

5) M. Tsujimoto, Y. Matsumoto, T. Tomita, A. Sakai, and S. Nakatsuji, Phy. Rev. Lett. **113**, 267001 (2014).

6) M. Date, J. Phys. Soc. Jpn. **39**, 892 (1975).

7) K. Kindo, J. Phys.: Conf. Ser. **51**, 522 (2006).

8) K. Kindo, Physica B **294-295**, 585-590 (2001).

9) L. Esaki, Phys. Rev. **109**, 603 (1958).

10) G. J. Athas, J. S. Brooks, S. J. Klepper, S. Uji, and M. Tokumoto, Rev. Sci. Instrum. **64**, 3248 (1993).

11) E. Ohmichi, E. Komatsu and T. Osada, Rev. Sci. Instrum. **75**, 2094 (2004).

12) M. M. Altarawneh, C. H. Mielke, and J. S. Brooks, Rev. Sci. Instrum. **80**, 066104 (2009).

13) D. Shoenberg, Magnetic Oscillations in Metals (Cambridge University Press, Cambridge, U.K., 1984).

14) I. J. Schoenberg, Quart. Appl. Math. **4**, pp. 45-99 and 112-141 (1946).

15) C. Herring Phys. Rev. **52**, 365 (1937).

16) C. O. Larson and W. L. Gordon, Phys. Rev. **156**, 703 (1967).

17) R. Peierls Z. Phys. **80**, 763 (1933).

18) Y. Shimura, M. Tsujimoto, A. Sakai, B. Zeng, L. Balicas, and S. Nakatsuji, J. Phys.: Conf. Ser. **592**, 012026 (2015).